SPACEBORNE SAR TOMOGRAPHY IN URBAN AREAS

Othmar Frey
Earth Observation &
Remote Sensing, ETH Zurich
Gamma Remote Sensing
Switzerland
Email: otfrey@ethz.ch

Irena Hajnsek
Earth Observation & Remote Sensing
ETH Zurich, Switzerland /
German Aerospace Center - DLR,
Germany

Urs Wegmuller
Gamma Remote Sensing
Switzerland

***Abstract*—Persistent scatterer interferometry relies on the assumption that only one dominant scatterer is present per range-azimuth resolution cell. If this criterion is not met the point target candidate is discarded during the iterative processing sequence. This one-scatterer assumption contrasts with the fact that in urban scenarios layover is an ubiquitous phenomenon, and, therefore two or even more scatterers per resolution cell occur frequently. SAR tomography has the potential to support persistent scatterer interferometry in urban areas by providing a means to identify and separate two scatterers in elevation direction. In this paper, we explore an interferometric stack consisting of 25 ENVISAT/ASAR SLC images over Bucharest using SAR tomography approaches combined with interferometric point target processing. Elevation profiles are extracted using beamforming and truncated singular value decomposition focusing approaches.**

***Index Terms*—Synthetic aperture radar (SAR), SAR tomography, SAR interferometry, persistent scatterer interferometry, interferometric stacking, spaceborne SAR**

I. INTRODUCTION

SAR tomography and differential SAR tomography are SAR imaging concepts that allow for a true three-dimensional and potentially even four-dimensional inversion of the spatiotemporal localization of scatterers. By exploiting the third imaging dimension SAR tomography adds valuable information about the structure of complex target scenarios thereby supporting a variety of SAR applications, such as forest parameter retrieval, structure information in urban areas, and retrieval of additional point targets in such scenarios. In SAR tomography, a large aperture is synthesized not only along-track, but also in elevation direction: By synthesizing an aperture from multiple repeated passes of the sensor, multiple backscattering sources that lie within one range-azimuth resolution cell can be resolved. In the spaceborne case, ideally 25 up to 50 or even 100 repeat-pass interferometric data sets of the same area with spatial baselines perpendicular to the line of sight are required to resolve targets also in the elevation direction, or potentially even in space and time.

While 3-D tomographic reconstruction from multibaseline SAR data has been demonstrated by a number of authors in different scenarios, such as urban areas [1]–[5] and forest environments [6]–[12], research and development is still required to bring the techniques to an operational level [13].

In this contribution, we explore an interferometric stack of ENVISAT/ASAR SLC images over Bucharest, Romania, by analyzing selected point targets using the tomographic inversion approaches: (1) beamforming and (2) truncated singular value decomposition (TSVD), and (3) singular value decomposition using Tikhonov regularization. The performance of the algorithms with respect to tomographic focusing of selected point targets is discussed.

II. DATA

The number of ENVISAT/ASAR SLCs $K = 25$ available in this stack is at the lower end of what is typically recommended for persistent scatterer processing. Note also, that the total time span between the acquisitions is roughly 6 years. In terms of favorable prerequisites for tomographic processing, this situation is non-ideal, however, it is a rather typical case occurring in PSI-based deformation extraction. In particular, covering a long time-series often is of advantage to extract slow deformation.

Fig. 1(a) shows the temporal and spatial baseline constellation of the interferometric stack. In Fig.1(b) the distribution of the point targets over the imaged scene is depicted. The pattern corresponds to unwrapped low frequency spatial variations of the interferometric phases which are attributed mainly to atmosphere and which are isolated during PSI processing.

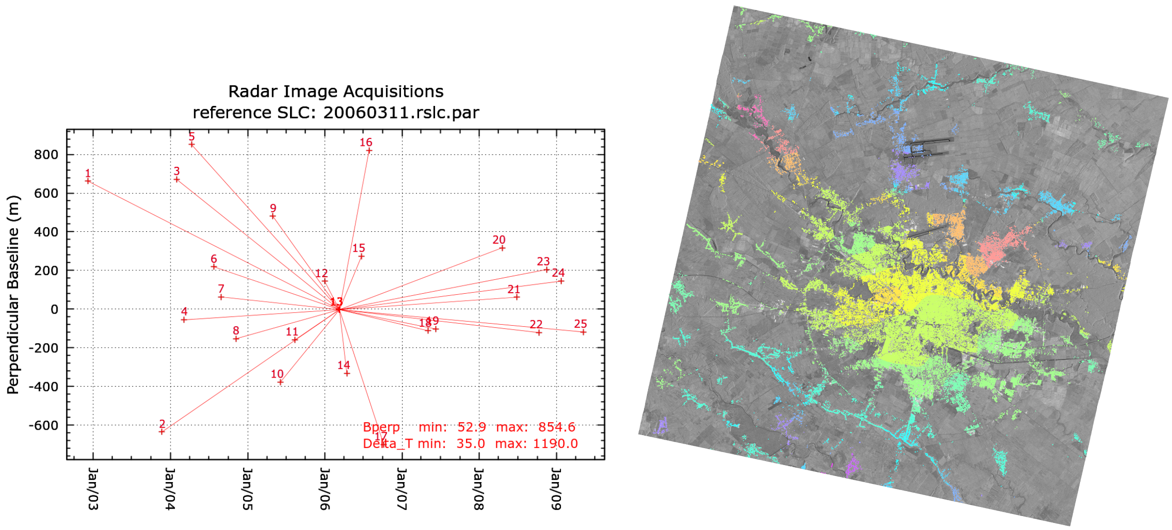

(a) (b)

Fig. 1. (a) Temporal and spatial perpendicular baseline components B_p of the interferometric stack of ENVISAT/ASAR SLC data (descending orbit no. 465) over Bucharest, Romania, with respect to a single reference. The distribution of B_p indicates the irregular sampling in the elevation direction. (b) Overlay of the atmospheric phase pattern estimated at point target locations and the geocoded averaged multi look intensity image. For each layer of the SLC stack atmospheric phase and deformation phase estimates are obtained from an initial PSI processing to provide a better phase calibration as a starting point for the tomographic processing.

For this data set, the approximate resolution δ_n that can be expected from tomographic focusing using beamforming in the elevation direction is $\delta_n = \frac{\lambda r}{2L} = 15.5m$, where $L = 1563.2m$ is the maximal length of the synthesized aperture in elevation direction. Accounting for the irregular sampling the unambiguous imaging extension in elevation direction is approximately $65 - 70m$.

III. Methods

Before tomographic imaging in the elevation direction is applied to the spaceborne interferometric stack, the data have to undergo a number of processing steps, essentially a PSI processing sequence, in order to isolate the atmospheric phase component [14]. The preprocessing steps include:

1) Selection of reference scene from stack of SLC images.
2) Geocoding using the multilook intensity image of the reference scene.
3) Coregistration including a refinement step using offset estimates between the data sets of the stack.

Then, persistent scatterer candidates are selected based on spectral diversity and the temporal variability of the backscattering. In a next step, point differential interferograms are obtained in an iterative manner. For each persistent scatterer candidate, the topographic and orbital phases are simulated and subtracted from the point-wise complex-valued interferogram followed by unwrapping and filtering in order to isolate the spatially correlated phase contributions from high-frequency phase contributions such as the residual topographic phase. Once an acceptable PSI solution is obtained, the tomographic focusing algorithms can be applied.

Estimators such as Capon and MUSIC rely on an ensemble average of the sample covariance matrix. While they permit to obtain a focused image in elevation direction, the resolution is decreased in range/and azimuth. Since, for now, we deal with a preselected set of point targets, beamforming and truncated singular value decomposition (TSVD) based tomographic focusing approaches are applied. These methods allow for tomographic processing without compromising the range and azimuth resolution through multilooking. The resulting location of the most prominent scatterers provides additional information about the localization of potential additional point target candidates.

In the following, the system model and the tomographic inversion approaches are briefly introduced. For a more comprehensive treatment of the subject the reader is referred to the respective references.

The complex reflectivity s of a point target source can be described as

$$s = \alpha e^{i\phi}, \tag{1}$$

where α is the amplitude and ϕ is the phase of s. So the complex demodulated signal vector $\mathbf{y}$ for that particular source s yields

$$\mathbf{y} = \mathbf{a}s \tag{2}$$

where $\mathbf{a} = [1\ e^{i\varphi_2} \dots e^{i\varphi_K}]^T$ is the steering vector with $\varphi_m = -2k_c(r_m - r_1)$, $m = 1 \dots K$; k_c is the central wavenumber and r_m is the range distance from the point scatterer to the m-th sensor position.

Then, for p point target sources the signal vector $\mathbf{y}$, which represents the signal impinging on the antenna array synthesized by the different locations of the various SLC acquisition in elevation direction is

$$\mathbf{y} = \begin{bmatrix}\mathbf{a}_1 & \dots & \mathbf{a}_p\end{bmatrix}\begin{bmatrix}s_1\\ \vdots \\ s_p\end{bmatrix} = \mathbf{B}\mathbf{s}. \tag{3}$$

The matrix $[\mathbf{a}_1 \dots \mathbf{a}_p]$ is summarized in matrix $\mathbf{B}$ called the steering matrix.

A straight-forward reconstruction—the beamforming case—of the complex reflectivity $\hat{\mathbf{s}}$ along the elevation direction is obtained by

$$\hat{\mathbf{s}} = \mathbf{B}^H\mathbf{y} \tag{4}$$

Since the sampling of the tomography data is non-uniform in the elevation direction the reconstructed profile is prone to spurious side lobes. A method that provides a regularized inversion is the truncated singular value decomposition (TSVD) approach as it has been suggested and applied in the context of SAR tomography in [15]. It starts with a singular value decomposition of the steering matrix $\mathbf{B} = \mathbf{U}\mathbf{\Sigma}\mathbf{V}^H$. Depending on the decay pattern of the singular values σ_n stored in the diagonal matrix Σ, a noise threshold is set at the Q-th singular value. All singular values $\sigma_n, n = Q+1, ..., K$ that lie below this threshold, as well as their corresponding orthogonal vectors $\mathbf{u}_n$, $\mathbf{v}_n$, are discarded. The inversion is then performed via the truncated pseudo-inverse $\mathbf{V}_{1,Q}(\mathbf{\Sigma}^{-1})_{1,Q}\mathbf{U}^H_{1,Q}$ of the steering matrix $\mathbf{B}$:

$$\hat{\mathbf{s}} = \mathbf{V}_{1,Q}(\mathbf{\Sigma}^{-1})_{1,Q}\mathbf{U}^H_{1,Q}\mathbf{y} \tag{5}$$

$\mathbf{B}$ is the steering matrix of size $K \times N_r$, where K is the number of acquisitions and N_r is the number of equally-spaced locations at which the profile in elevation direction is inverted.

Another approach to regularize the inversion is the Tikhonov-regularization. Instead of setting a threshold between signal and noise space, the inverse singular values $\sigma^{-1}_{n_{rt}}$ are weighted according to the following scheme

$$\sigma^{-1}_{n_{rt}} = \frac{\sigma_n}{\sigma_n^2 + \epsilon^2}, \tag{6}$$

where ϵ^2 is the noise power level. This method was reported to provide more stable performance in [5].

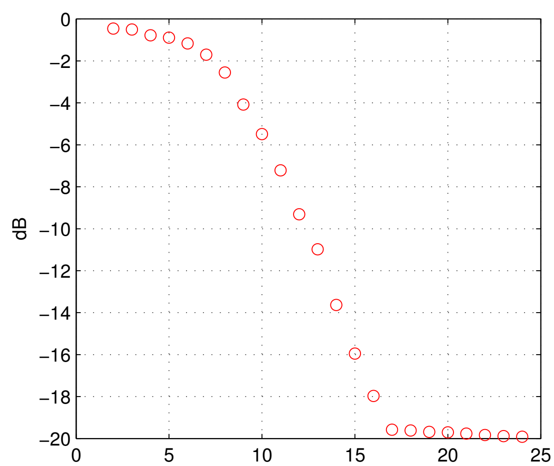

Fig. 2. Example of the decay of the singular values for a point target location taken from the ENVISAT/ASAR data stack.

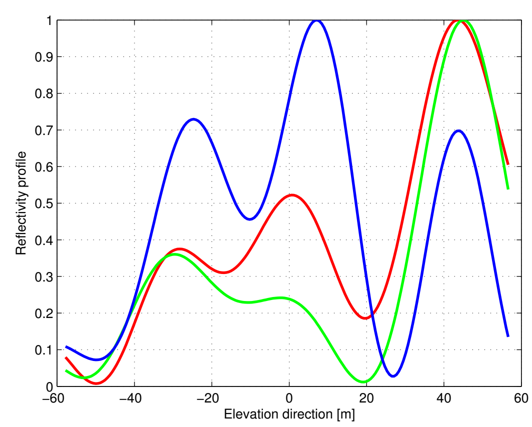

Fig. 3. Tomographic profile of reflectivity in elevation direction as estimated at the location of a selected point target from the ENVISAT/ASAR data stack over Bucharest. Red: beamforming, green: truncated singular value decomposition, blue: SVD using Tikhonov regularization. The singular value threshold is set to 6 for TSVD and also for the calculation of the weights for weighted SVD.

IV. Results

Fig. 2 shows the distribution of singular values obtained from the singular value decomposition of the steering matrix for a selected location that was previously selected as a point target in the PSI processing. In Fig. 3 tomographic profiles obtained from the inversion methods beamforming, TSVD, and SVD using Tikhonov regularization are given. It has to be noted that for the SVD based methods the noise floor has to be chosen carefully. Choosing the 6-th singular value as a threshold is not very obvious from examining Fig. 2. A noise floor starting from 17 seems to be more likely. However, the latter would lead to high-frequency disturbance of the reflectivity signal.

V. Discussion

Tomographic imaging in the elevation direction was applied to selected point targets previously obtained by PSI-processing of an interferometric stack over Bucharest, Romania. The focusing behavior using the beamforming and the truncated singular value decomposition as well as using Tikhonov-regularization was found to be rather unstable for the particular data set which consists of only 25 SLCs. The relatively low number of acquisitions together with the rather nonuniform sampling in elevation direction is suspected to be the cause. It is intended to further test these algorithms with different types (different sensors, number of SLCs, sampling) of spaceborne interferometric stacks in order to obtain a better picture of the potential and limitations with respect to the added-value for the interferometric point target processing of spaceborne SAR data, in particular for reliably separating multiple targets in one resolution cell.

Acknowledgment

This research project is funded by the Swiss Space Office, State Secretariat for Education and Research of the Swiss Confederation (SER/SSO), through the MdP2012 initiative. The ENVISAT/ASAR data used are provided courtesy of ESA. SRTM ©USGS.

References

[1] G. Fornaro and A. Pauciullo, “LMMSE 3-D SAR focusing,” *IEEE Trans. Geosci. Remote Sens.*, vol. 47, no. 1, pp. 214–223, Jan. 2009.

[2] G. Fornaro and F. Serafino, “Imaging of single and double scatterers in urban areas via sar tomography,” *IEEE Trans. Geosci. Remote Sens.*, vol. 44, no. 12, pp. 3497–3505, 2006.

[3] S. Sauer, L. Ferro-Famil, A. Reigber, and E. Pottier, “Three-dimensional imaging and scattering mechanism estimation over urban scenes using dual-baseline polarimetric InSAR observations at L-band,” *IEEE Trans. Geosci. Remote Sens.*, vol. PP, no. 99, pp. 1–14, 2011.

[4] D. Reale, G. Fornaro, A. Pauciullo, X. X. Zhu, and R. Bamler, “Tomographic imaging and monitoring of buildings with very high resolution SAR data,” *IEEE Geosci. Remote Sens. Lett.*, vol. 8, no. 4, pp. 661 –665, July 2011.

[5] X. X. Zhu and R. Bamler, “Very high resolution spaceborne SAR tomography in urban environment,” *IEEE Trans. Geosci. Remote Sens.*, vol. 48, no. 12, pp. 4296–4308, 2010.

[6] A. Reigber and A. Moreira, “First Demonstration of Airborne SAR Tomography Using Multibaseline L-Band Data,” *IEEE Transactions on Geoscience and Remote Sensing*, vol. 38, no. 5, pp. 2142–2152, 2000.

[7] O. Frey and E. Meier, “Analyzing tomographic SAR data of a forest with respect to frequency, polarization, and focusing technique,” *IEEE Trans. Geosci. Remote Sens.*, vol. 49, no. 10, pp. 3648–3659, Oct. 2011.

[8] O. Frey and E. Meier, “3-D time-domain SAR imaging of a forest using airborne multibaseline data at L- and P-bands,” *IEEE Trans. Geosci. Remote Sens.*, vol. 49, no. 10, pp. 3660–3664, Oct. 2011.

[9] O. Frey, F. Morsdorf, and E. Meier, “Tomographic Imaging of a Forested Area By Airborne Multi-Baseline P-Band SAR,” *Sensors, Special Issue on Synthetic Aperture Radar*, vol. 8, no. 9, pp. 5884–5896, sep 2008.

[10] E. Aguilera, M. Nannini, and A. Reigber, “Multisignal compressed sensing for polarimetric SAR tomography,” *IEEE Geosci. Remote Sens. Lett.*, vol. PP, no. 99, pp. 1–5, 2012.

[11] S. Tebaldini, “Single and multipolarimetric SAR tomography of forested areas: A parametric approach,” *IEEE Trans. Geosci. Remote Sens.*, vol. 48, no. 5, pp. 2375–2387, May 2010.

[12] M. Nannini, R. Scheiber, R. Horn, and A. Moreira, “First 3-d reconstructions of targets hidden beneath foliage by means of polarimetric sar tomography,” *IEEE Geoscience and Remote Sensing Letters*, vol. 9, no. 1, pp. 60 –64, jan. 2012.

[13] “Fringe 2011 sorted recommendations,” ESA, Frascati, Italy, Sept. 2011.

[14] U. Wegmuller, D. Walter, V. Spreckels, and C. Werner, “Nonuniform ground motion monitoring with terrasar-x persistent scatterer interferometry,” *Geoscience and Remote Sensing, IEEE Transactions on*, vol. 48, no. 2, pp. 895 –904, feb. 2010.

[15] G. Fornaro, F. Serafino, and F. Soldovieri, “Three-dimensional focusing with multipass sar data,” *IEEE Trans. Geosci. Remote Sens.*, vol. 41, no. 3, pp. 507–517, 2003.